Journal of Marine Science and Technology manuscript No.
(will be inserted by the editor)

Linear and Nonlinear Analyses of the Porpoising Dynamics of High-Speed Planing Craft Using Full-Scale Trial Data

Satoru Hamada · Atsuo Maki

Received: date / Accepted: date

Abstract Although it is known from previous studies that porpoising in high-speed planing craft is a Hopf bifurcation, this study examined its occurrence and disappearance using the motion model identified from full-scale test data. Herein, we first analyzed the stability of the system linearized near the equilibrium point. From its results, we reconfirmed the knowledge that porpoising occurs when the system becomes unstable in the vicinity of the equilibrium point. We also found that the system became unstable as the thrust or trim angle of the outboard motor decreased. This finding was consistent with the results of a full-scale craft test performed in a previous study. Second, we confirmed that the limit cycle which is a result of the nonlinearity of the system was stable. The two analyses indicate that porpoising corresponds to the supercritical Hopf bifurcation. Furthermore, in the vicinity of the bifurcation point, it was found that stable equilibrium points and stable limit cycles can coexist. Finally, we confirmed this phenomenon in the full-scale test.

Keywords High-speed boat · Planing hull · Porpoising · Nonlinear analysis · Hopf bifurcation

1 Introduction

The proportion of the boat equipped with the outboard motor has increased on behalf of the stern drive boat decrease due to the development of large-sized outboard motor and expansion of the use of multiple motors [1]. In addition, as the stepped hull craft gained widespread use, boats became faster. Because a stern drive requires the engine to be installed in the confined engine room, it is difficult to maintain and also takes up a lot of space inside the craft. Therefore, converting a stern drive to an outboard motor helps improve the maintainability and comfort of the boat. On the other hand, moving the engine to the stern increases the possibility of porpoising, a coupled heave and pitch motion [2].

System stability and the porpoising occurrence have been extensively researched. Savitsky [3] showed the limitation of porpoising using the experimental data from a prismatic planing hull conducted by Day and Haag [4]. Savitsky [3] calculated the attitude at which thrust, lift, and drag were balanced, and if the pitch angle of the craft was less than the porpoising limit, the craft remained stable. Based on the research of Savitsky [3] and Brown [5], Ekman and Rydelius [6] investigated the effect of the height of the interceptors on the porpoising limit. They added a constant value to the trim angle to match the result of the full-scale craft test. Hicks et al. [2] identified the limit position of the center of gravity of the craft by analyzing changes in stability by using a linearized system. They also showed that the occurrence or disappearance of porpoising depends on the quadratic terms that are included in the system in the nonlinear simulation. Katayama [7] identified the system parameters of a linear system through constraint tests and found that porpoising diminishes as the damping coefficients increase and that it disappears completely when the coupling restoring coefficients are removed. Sun and Faltinsen [8] identified the system parameters of a linear model using a 2D+t theory and a boundary element method. They estimated the occurrence of porpoising via a stability analysis using the identified linear system and calculated the time history using a nonlinear model. They also investigated the limit of porpoising based on the position of the center of gravity of the craft using numerical simulation based on the 2d+t theory [9]. They compared their results with those of the test conducted by

Satoru Hamada
Osaka University, 2-1 Yamadaoka, Suita, Osaka, Japan
Yamaha Motor Co., LTD. 2500 Shingai, Iwata, Shizuoka, Japan
E-mail: hamada_satoru@naoe.eng.osaka-u.ac.jp

Atsuo Maki
Osaka University, 2-1 Yamadaoka, Suita, Osaka, Japan

Day and Haag [4] and found that the critical position of the center of gravity of the craft determined by them was similar to the test result. Thus, many studies have investigated the relationship between the center of gravity and the occurrence of porpoising, recently, Zan et al. [10] investigated the effects of the center of gravity and moment of inertia on the occurrence of porpoising in trimaran boats, and showed that moving the center of gravity forward or increasing the moment of inertia increases the amplitude of porpoising. Some studies have also been found using computational fluid dynamics (CFD) to investigate with respect to the occurrence of porpoising. Kim et al. [11] investigated the occurrence of porpoising by considering the differences in the side appendages using CFD. Sajedi et al. [12] also investigated the hydrodynamic effects of wedges with different heights using experiments and CFD, and confirmed that wedging can reduce the phenomenon of porpoising.

Meanwhile, there are some studies that deal with the phenomenon of porpoising from the perspective of nonlinear dynamics. Troesch and Falzarano [13] showed that the occurrence and disappearance of porpoising is a Hopf bifurcation. Hopf bifurcation here is called a bifurcation phenomenon in which periodic solutions appear from an equilibrium state [14]. They investigated the stability of the linear system and further showed that Hopf bifurcation occurs when the center of gravity of the craft changes by using a nonlinear simulation based on the model test of the study by Troesch [15]. These studies showed that porpoising is caused by a loss of stability in the vicinity of the equilibrium point of the system and that limit cycles occur in nonlinear systems. We have not been able to find any reports on the stability of porpoising as a limit cycle in our paper survey. In addition, the aforementioned studies considered using a system based on model tests, and it is difficult to say whether they can reproduce the phenomena at the actual scale. Katayama et al. [16] estimated the lift, drag, and pitch moments on the actual scale using those obtained by a constrained model test. Using simulations, they found that the range of porpoising on the actual scale is greater than that estimated from the model scale. However, this finding was not verified by an actual scale test.

We proposed a numerical motion model of an outboard motor planing craft running straight and a system identification method based on full-scale test results [17,18]. In these studies, we obtained the system parameters including those for the nonlinear system by using covariance matrix adaptation evolution strategy (CMA-ES). The simulation result obtained using the nonlinear system was similar to the test result, and overall, it reproduced the porpoising phenomenon and the amplitude of pitch angle well. In the present research, we clarified the phenomenon of porpoising via bifurcation analysis in the nonlinear dynamical theory by analyzing the nonlinear system obtained from a full-scale test result and a linearized system in the vicinity of the equilibrium point.

This paper is organized as follows. In Section 2, we review our previous studies [17,18] and confirm the validity of the model used in this research. In Section 3, we explain the linearized method in the vicinity of the equilibrium point and stability criterion. We also describe the method to find fixed points and stability criterion of limit cycles. In Section 4, we present the analysis of the stability around the equilibrium point and the fixed point of the model identified in Section 2; further, we explain the occurrence of porpoising and bifurcation phenomena. Finally, Section 5 concludes this paper.

2 Motion model and system identification [17,18]

2.1 Coordinate system and motion equation

Porpoising can be described as a motion with three degrees of freedom: surge, heave, and pitch. A right-handed Cartesian coordinate system is used and the coordinate system is a space-fixed system $o-xz$. The forward direction along the horizontal plane is x; the downward direction is z; the upward rotating direction is θ. Fig. 1 shows the coordinate system, and each force and position acting on the craft and engine is defined in Tables 1 and 2. They duplicate fig. 1, tables 1 and 2 in the literature [18]. In the tables, CoG stands for center of gravity; CoT, for center of engine trim; and OoH, for the origin of the craft, which is defined as the intersection of the baseline and transom.

Table 1: List of forces and force points for an outboard motor planing craft. This table duplicates Table 1 in the literature [18].

Definition	Notation
Drag of craft w/o engine [N]	D_b
Vertical position of D_b from OoH [m]	H_D
Lift of craft w/o engine [N]	N_L
Longitudinal position of N_L [m]	L_L
Buoyancy [N]	N_B
Longitudinal position of N_B from OoH [m]	L_B
Longitudinal position of CoG from OoH [m]	L_CG
Vertical position of CoG from OoH [m]	H_CG
Sinkage of craft origin [m]	d
Wetted keel length [m]	L_K
Overall length of craft [m]	L_OA

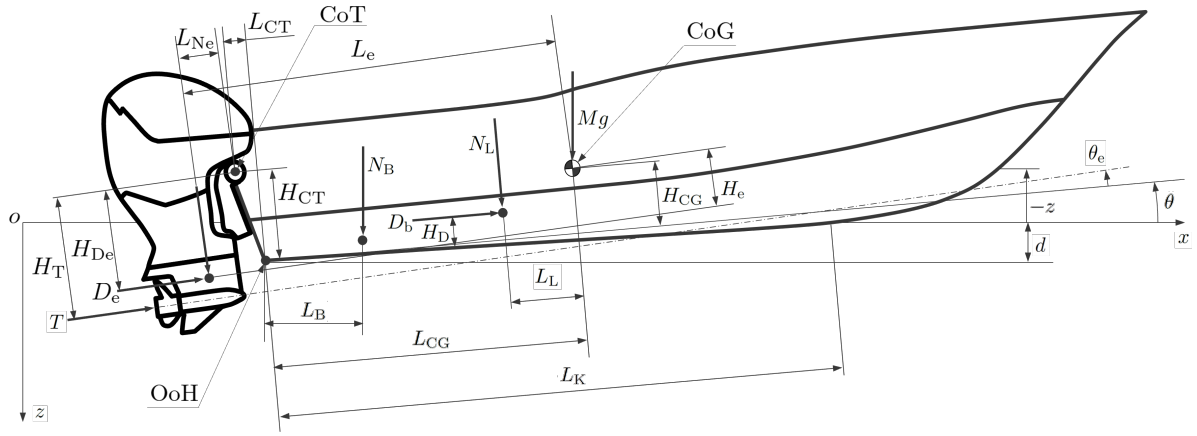

Fig. 1: Coordinate system and parameter definitions. This figure duplicates fig. 1 in the literature [18].

Table 2: List of forces and force points for the engine. This table duplicates Table 2 in the literature [18].

Definition	Notation
Thrust [N]	T
Vertical position of T from CoT [m]	H_T
Drag of engine [N]	D_e
Vertical position of D_e from CoT [m]	H_{De}
Vertical position of D_e [m]	H_e
Lift of engine [N] [m]	N_e
Longitudinal position of N_e from CoT [m]	L_{Ne}
Longitudinal position of N_e [m]	L_e
Longitudinal position of engine from OoH [m]	L_{CT}
Vertical position of engine from OoH [m]	H_{CT}

The motion equations derived using the defined forces and positions are as given in Eqs. (1) to (3).

$$\begin{aligned}(M + M_x)\,\ddot{x} &= D_b \cos\theta + (T + D_e)\cos(\theta + \theta_e) \\ &\quad + N_L \sin\theta + N_e \sin(\theta + \theta_e) \qquad (1)\\ (M + M_z)\,\ddot{z} &= -D_b \sin\theta - (T + D_e)\sin(\theta + \theta_e) \\ &\quad + N_L \cos\theta + N_e \cos(\theta + \theta_e) \\ &\quad + N_B + Mg - c_{zz}\dot{z} - c_{z\theta}\dot{\theta} \qquad (2)\\ (I_y + J_y)\,\ddot{\theta} &= D_b\,(H_{CG} - H_D) + T\,(H_T - H_{De} + H_e) \\ &\quad + D_e H_e + N_L L_L + N_e L_e \\ &\quad + N_B\,(L_{CG}\cos\theta - L_B) - c_{\theta z}\dot{z} - c_{\theta\theta}\dot{\theta} \qquad (3)\end{aligned}$$

Here, the overdot indicates the time derivative. M [kg] represents the total mass, including the mass of engine; M_x [kg] and M_z [kg] are the added masses in the x and z directions, and I_y [kgm^2] represents the moment of inertia in the pitch direction. J_y [kgm^2] is the added moment of inertia in the pitch direction. θ_e [°] represents the trim angle of the engine and c_{zz} [Ns/m], $c_{z\theta}$ [Ns], $c_{\theta z}$ [Ns], and $c_{\theta\theta}$ [Nms] are damping coefficients.

2.2 Study case

In this study, we considered the system stability of a planing craft with a 221 kW outboard motor; this craft and motor were the same as that used in our previous research [17, 18]. The specifications of the studied craft are given in Table 3, and this table also duplicates Table 5 in the literature [18].

Table 3: Principal particulars of the studied craft. This table duplicates Table 5 in the literature [18].

Item	Value
Weight of craft with engine: M [kg]	2709
Overall length of craft: L_{OA} [m]	7.09
Long. pos. of CoG: L_{CG} [m]	1.98
Vert. pos. of CoG: H_{CG} [m]	0.70
Long. pos. of engine from OoH: L_{CT} [m]	0.21
Vert. pos. of engine from OoH: H_{CT} [m]	0.69
Vert. pos. of T from CoT: H_T [m]	1.03
Long. pos. of Ne from CoT: L_{Ne} [m]	0.30
Vert. pos. of De from CoT: H_{De} [m]	1.03
Maximum speed of craft: $\dot{x}_{max}$ [m/s]	22.25

2.3 System identification with experimental data

In this study, we used the experimental data of Hamada et al. [17] for the identification of the nonlinear system. The experimental data were obtained by running the aforementioned craft twice at a fixed throttle with a given trim angle and engine speed. In previous studies, experimental data measured at 100 Hz were thinned to 50 Hz, but in this study, the 100 Hz experimental data were used as is. The experimental data are listed in Table 4.

Table 4: List of training and test data. The symbols ○ and ● represent the training and test data, respectively.

	$\theta_e = 4$	$\theta_e = 0$	$\theta_e = -2$	$\theta_e = -4$	$\theta_e = -8$
$10.0 \leq \dot{x} < 11.8$	○○	○○	○●	○●	-
$11.8 \leq \dot{x} < 13.0$	○●	○●	○○	○○	-
$13.0 \leq \dot{x} < 14.5$	○○	○○	○○	○●	○●
$14.5 \leq \dot{x} < 15.5$	○○	○●	○●	○○	○○
$15.5 \leq \dot{x} < 16.5$	-	-	-	-	○●
$16.5 \leq \dot{x} < 18.0$	○●	○○	○○	○●	○○
$18.0 \leq \dot{x} < 20.0$	○●	○●	○○	○○	○○
$20.0 \leq \dot{x} < 23.0$	○○	○○	○●	○○	○●

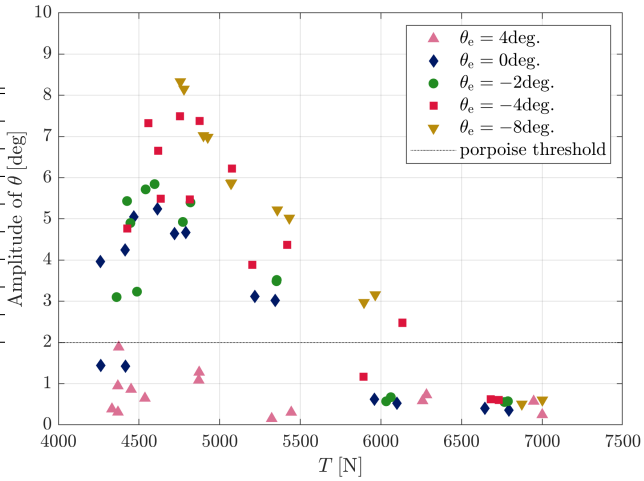

Fig. 2: Full-scale test result.

The columns give the range of $\dot{x}$ [m/s] for the θ_e [deg.] values in different rows. The craft speed is shown in ranges because it varies with the trim angle even for identical engine speed. The engine speed was basically set at every 250 rpm at low speed and every 500 rpm at high speed. The trim angle was basically set to in 4° increments and the center of the trim range, −2°, was additionally measured. When we perform system identification, we identify the system using a portion of the full-scale test result and examine the identified system using the rest of the result. We call the former data training data, which is marked with ○ in the table, and the latter data test data, which is marked with ●. The test data were randomly selected in the following manner.

- Three trial data were selected for each trim angle θ_e as test data.
- Two trial were selected for each speed range $\dot{x}$ as test data.

In this study, we needed to use a model to predict the occurrence or disappearance of porpoising. Therefore, the data, including conditions under which porpoising occurs and conditions under which it does not occur, were measured to identify the system. Fig. 2 shows the maximum pitch amplitude and thrust obtained by the full-scale test.

In the experiment, we characterized porpoising as a phenomenon that occurs when the pitch amplitude is larger than 2°. Among the 68 data listed in Table 4, porpoising occurs under 39 conditions and does not occur under 29 conditions. The amplitude of the pitch angle was greater at smaller trim angles, and as the speed decreased for the same trim angle, the amplitude of the pitch angle became greater. This means that the data can capture the change in porpoising occurrence with changes in craft speed and trim angle.

In the system identification process, we used CMA-ES, which is suitable for problems with a rugged search landscape including discontinuities. On the other hand, it should be noted that system identification requires a large amount of experimental data, as shown in Table 4. We modified some parameters from our previous work [17] as follows:

- initial value of λ was changed from 32 to 64.
- maximum value of λ was changed from 256 to 512.
- maximum iteration value was changed from 3×10^5 to 1×10^6.

Here, λ is the number of candidate solutions in CMA-ES. CMA-ES explores the optimal solutions by iterative computation, and the process will end at the maximum iteration value. Fig. 3 shows the pitch amplitude and thrust obtained by system identification using the data given in Table 4. The pitch amplitude of the calculation results is slightly smaller than that of the experimental results, but the occurrence and disappearance of porpoising are similar in both results.

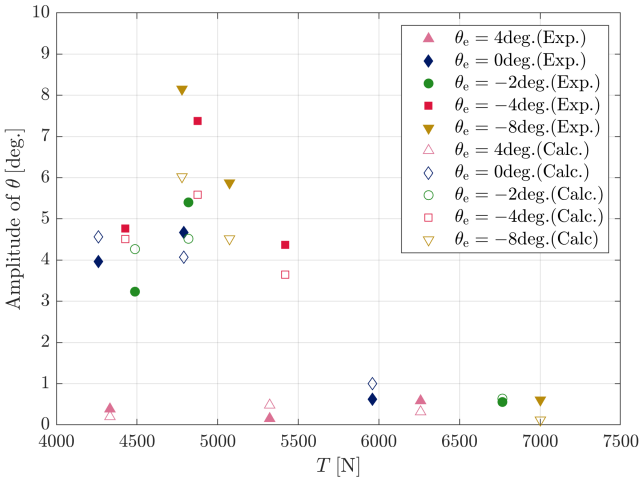

Fig. 3: System identification results. Here, "Exp." refers to the experimental results, and "Calc." refers to the calculated results obtained using the identified system.

3 Stability criterion of the equilibrium point and fixed point

3.1 Equilibrium point search and stability criterion

In this section, we first show how the equilibrium point is obtained. Then, we present a method to evaluate the stability of the equilibrium point by defining small perturbations from the equilibrium point. The state vector $X(t) \in \mathbb{R}^5$ and control vector $u(t) \in \mathbb{R}^2$ are defined as follows.

$$X(t) = \left[z(t)\ \theta(t)\ \dot{x}(t)\ \dot{z}(t)\ \dot{\theta}(t)\right]^T \tag{4}$$

$$u(t) = \left[T(t)\ \theta_e(t)\right]^T \tag{5}$$

Here, Eqs. (1) to (3) can be expressed as nonlinear state equations as follows.

$$\dot{X}(t) = \underbrace{\begin{bmatrix} f_1(X(t),\ u(t)) \\ f_2(X(t),\ u(t)) \\ f_3(X(t),\ u(t)) \\ f_4(X(t),\ u(t)) \\ f_5(X(t),\ u(t)) \end{bmatrix}}_{f(X,\ u)} \tag{6}$$

$f_1(X(t),\ u(t))$ to $f_5(X(t),\ u(t))$ are defined as follows.

$$f_1(X(t),\ u(t)) = \dot{z} \tag{7}$$

$$f_2(X(t),\ u(t)) = \dot{\theta} \tag{8}$$

$$\begin{aligned} f_3(X(t),\ u(t)) = \frac{1}{(M + M_x)} \{ & D_b \cos\theta \\ & + (T + D_e)\cos(\theta + \theta_e) + N_L \sin\theta \\ & + N_e \sin(\theta + \theta_e)\} \end{aligned} \tag{9}$$

$$\begin{aligned} f_4(X(t),\ u(t)) = \frac{1}{(M + M_z)} \{ & -D_b \sin\theta \\ & - (T + D_e)\sin(\theta + \theta_e) + N_L \cos\theta \\ & + N_e \cos(\theta + \theta_e) + N_B \\ & + Mg - c_{zz}\dot{z} - c_{z\theta}\dot{\theta}\} \end{aligned} \tag{10}$$

$$\begin{aligned} f_5(X(t),\ u(t)) = \frac{1}{(I_y + J_y)} \{ & D_b (H_{CG} - H_D) \\ & + T(H_T - H_{De} + H_e) + D_e H_e + N_L L_L \\ & + N_e L_e + N_B (L_{CG}\cos\theta - L_B) \\ & - c_{\theta z}\dot{z} - c_{\theta\theta}\dot{\theta}\} \end{aligned} \tag{11}$$

If the control vector is $u(t) = u^* = \text{const.}$, then the pair of $(X^*,\ u^*)$ defined by

$$f(X^*,\ u^*) = 0 \tag{12}$$

is called the equilibrium point. Here, * represents the parameters at the equilibrium point. We can uniquely find X^* using Eq. (12), given u^*. The minute deviation from the equilibrium point X^* is defined as $\xi(t) \in \mathbb{R}^5$. The orbit corresponding to this point can be described as follows:

$$X(t) = X^* + \xi(t) \tag{13}$$

Substituting Eq. (13) into Eq. (6) we get

$$\dot{X}(t) = \dot{X}^* + \dot{\xi}(t) = f(X^* + \xi(t),\ u^*) \tag{14}$$

If $\xi(t)$ is sufficiently small, we can apply the Taylor expansion for the right side and ignore terms higher than the second order.

$$f(X^* + \xi(t), u^*) = f(X^*, u^*) + \left.\frac{\partial f}{\partial X}\right|_{X(t)=X^*} \xi(t) \tag{15}$$

Since $X^* = \text{const.}$, $\dot{X}^*$ becomes 0. From Eqs. (12), (14) and (15), we can obtain the linear state equation regarding the equilibrium point X^* as follows.

$$\dot{\xi}(t) = \left.\frac{\partial f}{\partial X}\right|_{X(t)=X^*} \xi(t) \tag{16}$$

If $A \in \mathbb{R}^5$ is defined as

$$A = \left.\frac{\partial f}{\partial X}\right|_{X(t)=X^*} \tag{17}$$

and the eigenvalues of A are defined as λ_i^e, the equilibrium point is said to be stable if the following equation holds:

$$\mathrm{Re}\,\lambda_i^e < 0 \quad \forall i \tag{18}$$

3.2 Fixed point search and stability criterion

In a linearized system, when porpoising occurs, the origin is destabilized and the solution diverges for any initial value. On the other hand, in the actual phenomenon, the amplitude of porpoising eventually becomes stationary, and the limit cycle occurs because of the nonlinear nature of the system. To analyze the stability of the limit cycle, we employed Kawakami's method [19–21]. In this method, by using Newton's method for the nonlinear system, we can calculate not only the fixed point on the Poincaré section but also the characteristic multipliers of the Poincaré map. Then, the stability of the periodic orbit can be determined. This method is unique in that it can also compute unstable periodic orbits. In this section, we first show how this method can be used to search for a fixed point. Then we present a method to evaluate the stability of a fixed point by defining minute perturbations of the fixed point.

If the control vector $u = u_0 = \text{const.}$ is given, the orbit of Eq. (6) starting at $X = X_0$ and $t = t_0$ can be described as

$$X(t) = \varphi(t,\ X;\ t_0,\ X_0). \tag{19}$$

We use the following function:

$$q:\ \mathbb{R}^5 \to \mathbb{R};\ X(t) \mapsto q\left(X(t)\right) = \dot{\theta}(t) \tag{20}$$

The hypersurface Φ is defined as follows.

$$\Phi = \left\{X \in \mathbb{R}^5 \mid q\left(X(t)\right) = 0\right\} \tag{21}$$

Φ is the Poincaré section of φ. Since porpoising is the periodic motion with craft pitch angle θ, and since Eq. (19) denotes an oscillatory solution, $\varphi(t,\ X)$ will always intersect the hypersurface Φ. Now the variable Y and hypersurface Ψ are defined as follows.

$$Y(t) = \left[z(t)\ \theta(t)\ \dot{x}(t)\ \dot{z}(t)\right]^T \tag{22}$$

$$\Psi = \left\{Y \in \mathbb{R}^4\right\} \tag{23}$$

The map $\mathcal{H}$ from Φ to Ψ is defined as follows.

$$\mathcal{H}:\ \Phi \to \Psi;\ X \mapsto Y \tag{24}$$

Here, the crossing point between periodic solution and Φ is X_0, and Y_0 is $Y_0 = \mathcal{H}(X_0)$. For $Y_1 \in \Psi$, which is the neighborhood point of $Y_0 \in \Psi$, the point where $\varphi(t,\ X;\ t_0,\ X_1)$ whose initial value is $\mathcal{H}^{-1}(Y_1) = X_1 \in \Phi$ intersects Φ again is X_2, and the time is $t_0 + \tau(X_1)$. Then, X_2 is obtained as follows.

$$X_2 = \varphi\left(t_0 + \tau(X_1),\ X;\ t_0,\ X_1\right) \tag{25}$$

The map $\mathcal{P}$ from Ψ to itself using φ is defined as follows.

$$\mathcal{P}:\ \Psi \to \Psi;\ Y_1 \mapsto Y_2 = \mathcal{H}\big(\varphi\big(t_0 + \tau\left(\mathcal{H}^{-1}(Y_1)\right),\ X;\ t_0,\ \mathcal{H}^{-1}(Y_1)\big)\big) \tag{26}$$

If $X_0 \in \mathbb{R}^5$ satisfies the following equation,

$$\mathcal{H}^{-1}\left(\mathcal{P}\left(\mathcal{H}(X_0)\right)\right) = X_0, \tag{27}$$

X_0 is called the fixed point and $\tau_0 = \tau\left(\mathcal{H}^{-1}(Y_0)\right)$ is the period.

Next, the variable $\hat{X}$ is defined as follows.

$$\hat{X} = \left[z\ \theta\ \dot{x}\ \dot{z}\ \tau(X)\right]^T \tag{28}$$

The fixed point can be obtained by solving the following equation using Newton's method.

$$F(\hat{X}) = \varphi\left(t_0 + \tau(X_0),\ X;\ t_0,\ X_0\right) - X_0 = 0 \tag{29}$$

Jacobian matrix $J_{\mathrm{F}} \in \mathbb{R}^{5\times5}$ is defined as shown in the following equation.

$$J_{\mathrm{F}} = \frac{\mathrm{d}F}{\mathrm{d}\hat{X}} \tag{30}$$

By solving the difference equation,

$$\hat{X}^{(\hat{k}+1)} = \hat{X}^{(\hat{k})} - \alpha J_{\mathrm{F}}^{-1} F(\hat{X}^{(\hat{k})}) \tag{31}$$

until the end condition,

$$\|F(\hat{X}^{(\hat{k})})\| < \epsilon_{\mathrm{F}} \tag{32}$$

we get $\hat{X}$, which follows $F(\hat{X}) = 0$. Here, $\|F\|$ denotes the Euclidean norm. In this study, we defined $\epsilon_{\mathrm{F}} = 10^{-10}$. We set the initial value of α as 0.1 and used the damped Newton's method.

$$\|F(\hat{X}^{(\hat{k}+1)})\| < \|F(\hat{X}^{(\hat{k})})\| \tag{33}$$

If Eq. (33) is not satisfied, the value of α is multiplied by 0.5, and the procedure is repeated until the equation is satisfied. The orbit $\varphi(t,\ X;\ t_0,\ X_0)$ can be expressed in terms of its components as follows.

$$\varphi(t,\ X;\ t_0,\ X_0) = \begin{bmatrix} \varphi_1(t,\ X;\ t_0,\ X_0) \\ \varphi_2(t,\ X;\ t_0,\ X_0) \\ \varphi_3(t,\ X;\ t_0,\ X_0) \\ \varphi_4(t,\ X;\ t_0,\ X_0) \\ \varphi_5(t,\ X;\ t_0,\ X_0) \end{bmatrix} \tag{34}$$

We define the partial derivative of each component of X with respect to φ as follows.

$$\beta_{\mathrm{ij}} = \frac{\partial\varphi_{\mathrm{i}}(t_0 + \tau(X_0),\ X;\ t_0,\ X_0)}{\partial\hat{X}_{\mathrm{j}}}, \quad \text{for } i = 1,\cdots,5,\ j = 1,\cdots,5 \tag{35}$$

J_{F} stands for the following.

$$J_{\mathrm{F}} = \begin{bmatrix} \beta_{11}-1 & \beta_{12} & \beta_{13} & \beta_{14} & \beta_{15} \\ \beta_{21} & \beta_{22}-1 & \beta_{23} & \beta_{24} & \beta_{25} \\ \beta_{31} & \beta_{32} & \beta_{33}-1 & \beta_{34} & \beta_{35} \\ \beta_{41} & \beta_{42} & \beta_{43} & \beta_{44}-1 & \beta_{45} \\ \beta_{51} & \beta_{52} & \beta_{53} & \beta_{54} & \beta_{55} \end{bmatrix} \tag{36}$$

Finally, we consider the stability of the fixed point. The minute deviation from the fixed point is defined as $\delta^{(k)} \in \mathbb{R}^4$.

$$Y^{(k)} = Y_0 + \delta^{(k)} \tag{37}$$

Here, $Y^{(k+1)}$ can be expressed as follows.

$$Y^{(k+1)} = Y_0 + \delta^{(k+1)} = \mathcal{P}\left(Y_0 + \delta^{(k)}\right) \tag{38}$$

If $\delta^{(k)}$ is sufficiently small, we can perform the Taylor expansion of the right side of Eq. (38) and ignore terms beyond the second order.

$$\begin{aligned}\mathcal{P}\left(Y_0 + \delta^{(k)}\right) &= \mathcal{P}\left(Y_0\right) + \left.\frac{\mathrm{d}\mathcal{P}}{\mathrm{d}Y}\right|_{Y=Y_0} \delta^{(k)} \\ &= Y_0 + \left.\frac{\mathrm{d}\mathcal{P}}{\mathrm{d}Y}\right|_{Y=Y_0} \delta^{(k)}\end{aligned} \tag{39}$$

The following equation can be obtained from Eqs. (38) and (39).

$$\delta^{(k+1)} = \left.\frac{\mathrm{d}\mathcal{P}}{\mathrm{d}Y}\right|_{Y=Y_0} \delta^{(k)} \tag{40}$$

Here, the Jacobian matrix $J_\mathrm{S} \in \mathbb{R}^{4\times4}$ is defined as follows.

$$J_\mathrm{S} = \left.\frac{\mathrm{d}\mathcal{P}}{\mathrm{d}Y}\right|_{Y=Y_0} \tag{41}$$

Eq. (40) is the variational equation for the fixed point Y_0, and the stability of the fixed point can be distinguished by eigenvalues of J_S. Since the eigenvalues of J_S are defined as $\lambda_\mathrm{i}^\mathrm{f}$, the fixed point is stable if the following equation holds, i.e., if the eigenvalues are within the unit circle.

$$\|\lambda_\mathrm{i}^\mathrm{f}\| < 1 \quad \forall \mathrm{i} \tag{42}$$

These eigenvalues are called characteristic multipliers. From Eq. (26), we can derive the following equation.

$$\mathcal{P}(Y) = \mathcal{H}\left(\varphi(t_0 + \tau(X),\ X;\ t_0,\ X_0)\right) \tag{43}$$

By substituting this equation into Eq. (41), we get the following equation.

$$J_\mathrm{S} = \frac{\mathrm{d}\mathcal{H}\left(\varphi(t_0 + \tau(X),\ X;\ t_0,\ X_0)\right)}{\mathrm{d}Y} \tag{44}$$

If we expand this equation using β_ij, we obtain the following.

$$J_\mathrm{S} = \begin{bmatrix} \beta_{11} & \beta_{12} & \beta_{13} & \beta_{14} \\ \beta_{21} & \beta_{22} & \beta_{23} & \beta_{24} \\ \beta_{31} & \beta_{32} & \beta_{33} & \beta_{34} \\ \beta_{41} & \beta_{42} & \beta_{43} & \beta_{44} \end{bmatrix} \tag{45}$$

Thus, we can get J_F and J_S by using β_ij, and we can search for the fixed point and obtain the characteristic multipliers simultaneously.

4 Results and discussion

4.1 Stability in the vicinity of the equilibrium point

We calculated the stability of the equilibrium point of the system. Troesch and Falzarano [13] analyzed the occurrence of porpoising in relation to the center of gravity position. We focused on the input from the outboard motor and investigated how the stability of the equilibrium point changes with respect to changes in the trim angle and thrust of the outboard motor. Fig. 4 represents the relationship between craft speed $\dot{x}$ and thrust T at the equilibrium point of representative trim angles θ_e. The stability criterion at each point was obtained using Eq. (18).

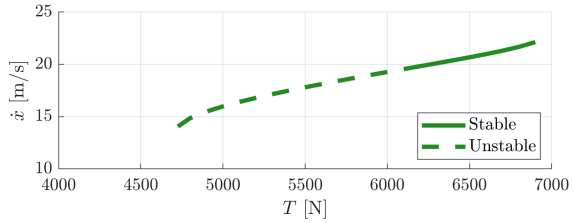

(a) Calculation result at $\theta_\mathrm{e} = -8°$.

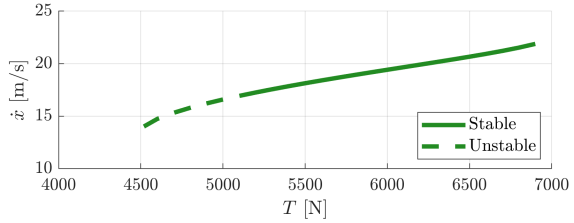

(b) Calculation result at $\theta_\mathrm{e} = -2°$.

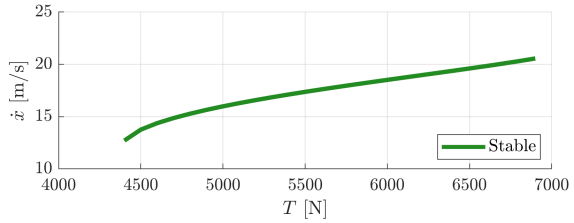

(c) Calculation result at $\theta_\mathrm{e} = 4°$.

Fig. 4: Velocity of the craft at each equilibrium point. The solid line represents stable states, and the dashed line represents unstable states.

The eigenvalues of the results corresponding to $\theta_\mathrm{e} = -2°$ are shown in Fig. 5. Each eigenvalue is identified as being on either the left half plane or the right half plane and is plotted on the complex plane.

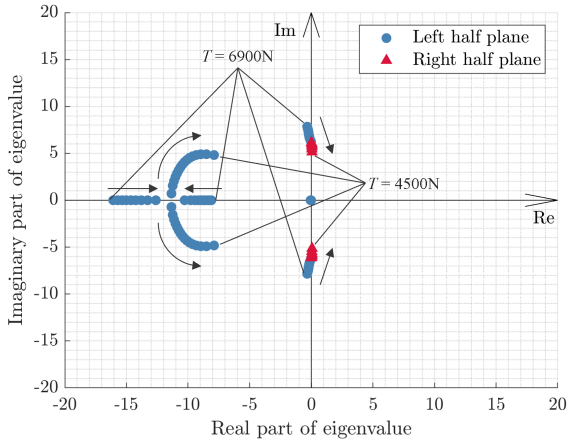

Fig. 5: Eigenvalues at $\theta_e = -2^\circ$ on the complex plane.

The eigenvalues were categorized into three groups: group $\mathcal{A}$ contained the eigenvalues around the origin point, while $\mathcal{B}$ comprised the complex conjugate eigenvalues around the imaginary axis, and $\mathcal{C}$ contained the complex conjugates or two real eigenvalues with high damping. The arrows indicate the change in eigenvalues with thrust for $\mathcal{B}$ and $\mathcal{C}$ groups; for $\mathcal{A}$, there is hardly any change with thrust. As the thrust decreased, i.e., as the speed of the craft decreased, the eigenvalues associated with $\mathcal{B}$ shifted to the right half-plane, indicating that the system was becoming unstable. Fig. 6 shows the stability of the equilibrium point with respect to T and θ_e. The stability analysis result in the vicinity

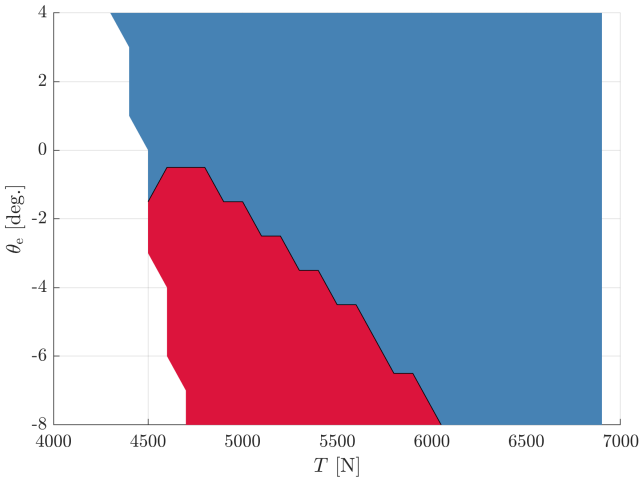

Fig. 6: Stability around the equilibrium point with varying thrust and trim angle. The blue area is determined as stable, and the red area is determined as unstable. The white area is an unexplored region.

of the equilibrium point confirmed that the instability of the region and the probability of porpoising occurrence would increase as the outboard trim angle decreases. This result is consistent with the tendency for the pitch angle amplitude to increase with decreasing outboard trim angle, as seen in Fig. 3.

4.2 Stability at the fixed point

The pitch angle amplitude θ_{amp} is defined as the amplitude of the orbit $\varphi_2\left(t \in \left[t_0,\ t_0 + \tau_0\right],\ X;\ t_0,\ X_0\right)$ calculated from the fixed point obtained by the method explained in Section 3.2. Fig. 7 shows the result of θ_{amp} with respect to T.

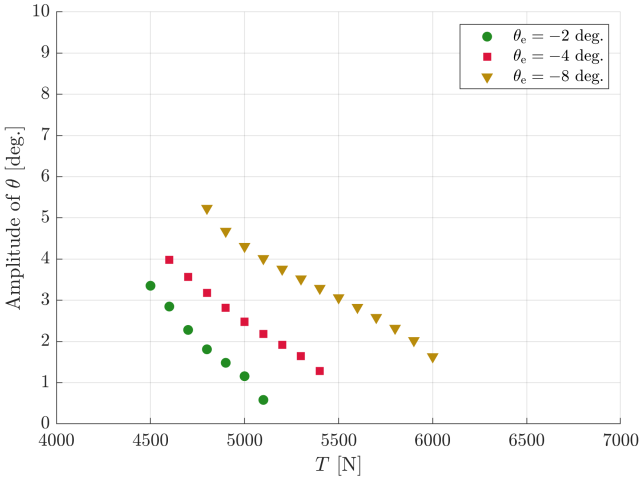

Fig. 7: Amplitude of θ over the time history of numerical simulation from the fixed point.

Although the absolute values were smaller compared to the value shown in Fig. 2, the tendency of the amplitude to increase as θ_e decreases, and the tendency of the amplitude to decrease as T increases were consistent. The stability at each point was also determined, and the system was found to be stable at all points. Fig. 8a shows the orbit of θ and $\dot{\theta}$ in $\varphi\left(t \in \left[t_0,\ t_0 + \tau_0\right],\ X;\ t_0,\ X_0\right)$ computed by the Euler method with time steps $\tau_0/1000$ s = 0.00116 s. In the figure, the red point indicates the fixed point at $\theta_e = -2^\circ$ and $T = 4600$ N. The light pink point indicates the point 0.1° added to θ of the fixed point, and the green point indicates the point -0.1° added to θ of the fixed point. Each colored line represents an orbit from the corresponding colored point. Fig. 8b shows a magnified view of Fig. 8a around the fixed point. Even if a disturbance is applied to the fixed point, the orbit asymptotically approaches the orbit with the fixed point as the initial value, indicating that the fixed point is stable.

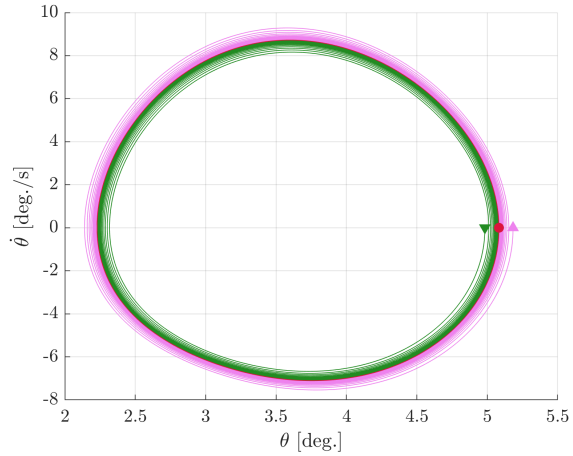

(a) Overall view.

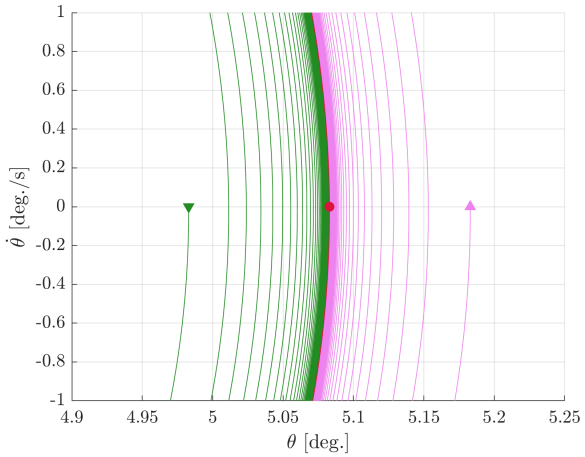

(b) Magnified view around the fixed point.

Fig. 8: Phase space of θ and $\dot{\theta}$. The red line is the orbit starting from the fixed point indicated by the red point. The pink line represents the orbit starting from the point obtained by adding 0.1° to θ of the fixed point. The green line represents the orbit starting from the point obtained by adding -0.1° to θ of the fixed point.

Fig. 9 shows the average craft speed of $\varphi_3\left(t \in \left[t_0,\ t_0+\tau_0\right], X; t_0, X_0\right)$ and the craft speed at equilibrium point with respect to T.

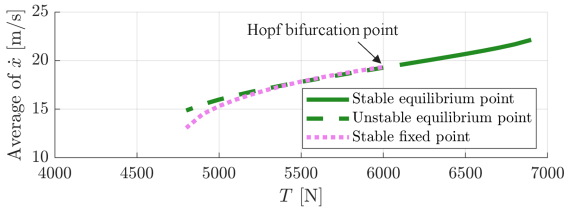

(a) Calculation result at $\theta_e = -8^\circ$.

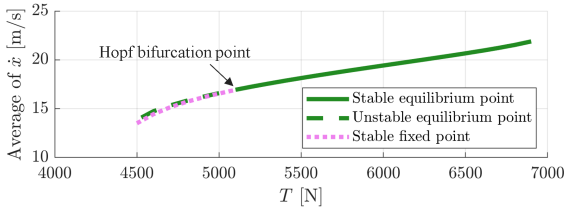

(b) Calculation result at $\theta_e = -2^\circ$.

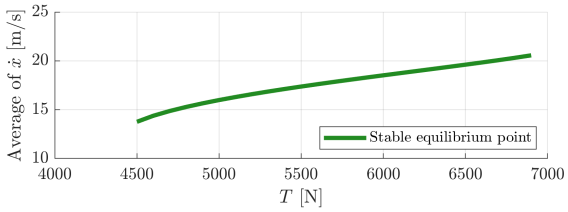

(c) Calculation result at $\theta_e = 4^\circ$.

Fig. 9: Velocity of the craft at the equilibrium point and average velocity at the fixed point. The solid green line represents stable equilibrium points, while the dashed green line represents unstable equilibrium points, and the dotted pink line represents fixed points.

The craft speed at the equilibrium point is the same as that shown in Fig. 4. As the thrust was gradually reduced, at some point, the equilibrium point became unstable, and simultaneously, a stable fixed point appeared. Porpoising occurred because of supercritical Hopf bifurcation, which was consistent with the phenomenon in the real craft where a change in craft speed causes a transition from a stable state to an unstable state, thereby resulting in a stable limit cycle, i.e., porpoising. On the other hand, although there are some research examples in the field of ship roll motion and capsizing that show the existence of heteroclinic points involved in a chaotic behavior [22], no such other bifurcation phenomena were observed in this study.

At the point $\theta_e = -2^\circ$ and $T = 5100$ N, the equilibrium point was stable, and a stable fixed point was also observed. To discuss this situation, we show the orbits from the fixed point and the equilibrium point under this condition in Fig. 10.

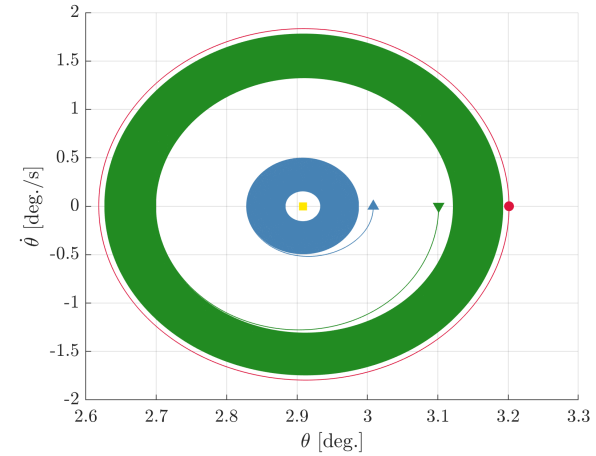

(a) Phase space of θ and $\dot{\theta}$.

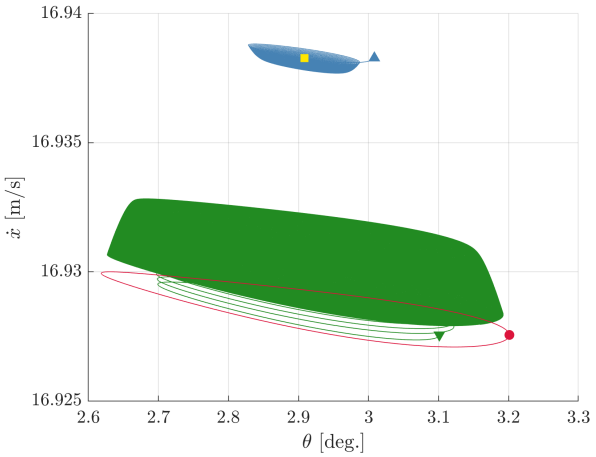

(b) Phase space of θ and $\dot{x}$.

Fig. 10: The orbits from the fixed point, the equilibrium point, and the points in the vicinity of both points. The red line indicates an orbit starting from the fixed point represented by the red point. The green line is the orbit starting from the point obtained by adding -0.1° to θ of the fixed point. The yellow point represents the equilibrium point. The blue line is the orbit starting from the point obtained by adding 0.1° to θ of the equilibrium point.

In each figure, the red and yellow points indicate the fixed and equilibrium points, respectively. The green point represents the point obtained by adding -0.1° to θ of the fixed point, and the blue point represents the point obtained by adding 0.1° to θ of the equilibrium point. Each colored line is the orbit from the corresponding colored point. These orbits were computed using the Euler method. The calculation time step of the red and green lines was $\tau_0/1000$ s $= 0.00101$ s and that of the blue line was 0.00010 s. The blue line converges to the point of equilibrium point marked in yellow, and the green line converges to the trajectory with the fixed point as the initial value, marked by the red line. From Fig. 10b, we could see that the craft speeds at the equilibrium point and fixed point were slightly different and that the state to which the system converged varied depending on the initial values even under identical input conditions.

4.3 Full-scale test

In the full-scale craft test, we observed that even a small disturbance could cause the craft to transition from a stable state without any porpoising to a state with porpoising and that a stable equilibrium point and a stable limit cycle could coexist in the vicinity of the bifurcation point. Fig. 11 shows the full-scale craft test results with $\theta_e = 4^\circ$ and $T = 4800$ N. The input conditions shown in Fig. 11 were different from those shown in Fig. 10; however, even if the input conditions did not change, no porpoising occurred up to 35 s, while porpoising occurred for 35 s and beyond. Thus, in the full-scale craft, even a small disturbance caused a transition from a state of stable running without porpoising to a state with porpoising, a stable equilibrium point and stable limit cycle coexisted near the bifurcation point. This also suggests that a slight change in state may be able to suppress porpoising, especially near the bifurcation point. The discussion of the dependence of initial values is a topic that is also covered in non-linear dynamics textbooks [23], and this is one of the examples. It is noteworthy that this could be observed in full-scale tests. The dependence on the initial value is a subject for future research.

5 Conclusion

Generally, systems identified by model experiments or CFD studies are used to study the conditions under which porpoising occurs. However, in this study, we performed bifurcation analysis on a model identified using full-scale craft test data. We observed that as the thrust on the craft was reduced, the equilibrium point became unstable, and the limit cycle occurred simultaneously. This limit cycle was stable, and supercritical Hopf bifurcation occurred at the bifurcation point. This phenomenon was consistent with the fact that in the full-scale craft, a stable limit cycle, i.e., porpoising, occurs when the speed of the craft is reduced. On the other hand, it was also found that near the bifurcation point, stable equilibrium point and stable limit cycle can coexist, and the converged state depends on the initial value. The exploration of this topic is one of our future research. In addition, we will investigate a control method that stabilizes unstable porpoising in the vicinity of the equilibrium point by controlling the trim angle of the outboard motor in the future.

Acknowledgements The authors would like to thank the referees for their detailed comments, helpful advice, and suggestions. Experiments

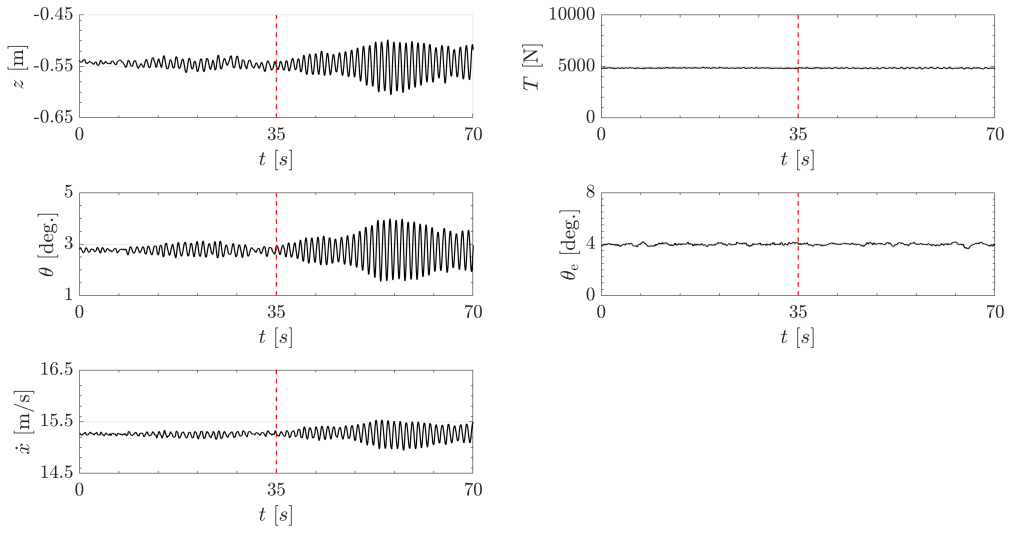

Fig. 11: Full-scale craft test results at $\theta_e = 4°$ and $T = 4800$ N. The dashed red line indicates 35 s.

for this study were conducted by Mr. Yasushi Iriono of Yamaha Motor Co., LTD. We would like to express our gratitude to Professor Naoya Umeda of Osaka University, Professor Toru Katayama of Osaka Metropolitan University and Professor Hiroyuki Kajiwara of Nagasaki Institute of Applied Science for their helpful discussions. We also thank Mr. Akihiro Onoue, Mr. Toshio Suzuki, Mr. Masaru Suemori, Mr. Yoshiyuki Kadobayashi, Mr. Shintarou Futagwa of Yamaha Motor Co., LTD., and Ms. Manami Oyama of YAMAHA MOTOR ENGINEERING CO., LTD. for continuous discussions. We are grateful to Enago (http://www.enago.jp) for reviewing the English language.

Conflict of interest

The authors declare that they have no conflict of interest.

References

1. National Marine Manufactures Association, 2020 powerboat sales trends. Tech. rep., National Marine Manufactures Association (2021). URL https://www.nmma.org/statistics/publications/statistical-abstract. Access at 2022/1/26.
2. J.D. Hicks, A.W. Troesch, C. Jiang, Simulation and Nonlinear Dynamics Analysis of Planing Hulls, Journal of Offshore Mechanics and Arctic Engineering **117**(1), 38 (1995)
3. D. Savitsky, Hydrodynamic Design of Planing Hulls, Marine Technology and SNAME News **1**(04), 71 (1964)
4. J.P. Day, R.J. Haag, Planing Boat Porpoising, Thesis, Webb Institute of Naval Architecture (1952)
5. P.W. Brown, An experimental and theoretical study of planing surfaces with trim flaps, Stevens Institute of Technology, Davidson Laboratory, Hoboken, New Jersey, USA, Report No. SIT-DL-71-1463 (1971)
6. F. Ekman, F. Rydelius. Model for Predicting Resistance and Running Attitude of High-Speed Craft Equipped with Interceptors : A comparative study including validation on Swedish Coast Guard patrol boat KBV 315 (2016)
7. T. Katayama, Mechanism of porpoising instabilities for high-speed planing craft. in *The Sixth ISOPE Pacific/Asia Offshore Mechanics Symposium* (OnePetro, 2004)
8. H. Sun, O. Faltinsen, Porpoising and dynamic behavior of planing vessels in calm water, 9th International Conference on Fast Sea Transportation, FAST 2007 pp. 396–404 (2007)
9. H. Sun, O. Faltinsen, Predictions of porpoising inception for planing vessels, Journal of Marine Science and Technology **16**, 270 (2011)
10. L. Zan, H. Sun, S. Lu, J. Zou, L. Wan, Experimental Study on Porpoising of a High-Speed Planing Trimaran, Journal of Marine Science and Engineering **11**(4) (2023)
11. S.W. Kim, K.C. Seo, D.K. Lee, G.W. Lee, A Numerical Study on Dynamic Instability Motion Control of Wave-Piercing High-Speed Planing Craft in Calm Water using Side Appendages, Journal of the Korean Society of Marine Environment & Safety **23**(3), 320 (2017)
12. S.M. Sajedi, P. Ghadimi, M. Sheikholeslami, M.A. Ghassemi, Experimental and numerical analyses of wedge effects on the rooster tail and porpoising phenomenon of a high-speed planing craft in calm water, Proceedings of the Institution of Mechanical Engineers, Part C: Journal of Mechanical Engineering Science **233**(13), 4637 (2019)
13. A.W. Troesch, J.M. Falzarano, Modern Nonlinear Dynamical Analysis of Vertical Plane Motion of Planing Hulls, Journal of Ship Research **37**(03), 189 (1993)
14. B.D. Hassard, N.D. Kazarinoff, Y.H. Wan, *Theory and applications of Hopf bifurcation*, vol. 41 (CUP Archive, 1981)
15. A.W. Troesch, On the Hydrodynamics of Vertically Oscillating Planing Hulls, Journal of Ship Research **36**(04), 317 (1992)
16. T. Katayama, T. Taniguchi, K. Habara, Tank tests to estimate the onset of dynamic instabilities of high-speed planing craft, Transactions - Society of Naval Architects and Marine Engineers **118**, 106 (2011)
17. S. Hamada, Y. Miyauchi, N. Umeda, A. Maki, 2022A-OS1-8 System identification of High Speed Planing Craft Using Full Scale Trial Data, Conference Proceedings The Japan Society of Naval Architects and Ocean Engineers **35**, 67 (2022)

18. S. Hamada, Y. Miyauchi, Y. Akimoto, N. Umeda, A. Maki, System identification of porpoising dynamics of high-speed planing craft using full scale trial data, Ocean Engineering **270**, 113585 (2023)
19. H. Kawakami, T. Matsumura, K. Kobayashi, An algorithm to obtain the periodic solutions on autonomous systems, Trans. Inst. Elec. Comm. Eng. Japan **61**(10), 1051 (1978)
20. H. Kawakami, Bifurcation of periodic responses in forced dynamic nonlinear circuits: Computation of bifurcation values of the system parameters, IEEE Transactions on Circuits and Systems **31**(3), 248 (1984)
21. K. Tsumoto, T. Ueta, T. Yoshinaga, H. Kawakami, Bifurcation analyses of nonlinear dynamical systems: From theory to numerical computations, Nonlinear Theory and Its Applications, IEICE **3**(4), 458 (2012)
22. A. Maki, Y. Miino, N. Umeda, M. Sakai, T. Ueta, H. Kawakami, Nonlinear dynamics of ship capsizing at sea, Nonlinear Theory and Its Applications, IEICE **13**(1), 2 (2022)
23. Y.A. Kuznetsov, *Elements of applied bifurcation theory*, vol. 112 (Springer, 1998)